Wind and Structures, Vol. 11, No. 3 (2008) 241-256
DOI: http://dx.doi.org/10.12989/was.2008.11.3.241

Wind velocity simulation of spatial three-dimensional fields based on autoregressive model

Wei-cheng Gao* and Yan-lei Yu‡

Department of Astronautic Science and Mechanics, Harbin Institute of Technology, Harbin, China
(Received November 5, 2007, Accepted May 22, 2008)

Abstract. This paper adopts autoregressive (AR) model to simulate the wind velocity of spatial three-dimensional fields in accordance with the time and space dependent characteristics of the 3-D fields. Based on the built MATLAB programming, this paper discusses in detail the issues of the AR model deduced by matrix form in the simulation and proposes the corresponding solving methods: the over-relaxation iteration to solve the large sparse matrix equations produced by large number of degrees of freedom of structures; the improved Gauss formula to calculate the numerical integral equations which integral functions contain oscillating functions; the mixed congruence and central limit theorem of Lindberg-Levy to generate random numbers. This paper also develops a method of ascertaining the rank of the AR model. The numerical examples show that all those methods are stable and reliable, which can be used to simulate the wind velocity of all large span structures in civil engineering.

Keywords: wind velocity; AR model; model rank; random numbers

1. Introduction

The fluctuating wind loads, which are related to the shape and height of the structure, are multiple-points random loads and one of the main dominating loads of the large structures in civil engineering. In the study on the wind-induced effects of the structure, the wind velocity is indispensably considered, but to obtain an accurate wind velocity model usually needs expensive cost through a full-ruler observation or a wind tunnel experiment. Therefore, it is significant to study the wind velocity simulation by numerical simulation methods.

The AR model was applied widely to forecast the time series in the wind engineering, because of its many merits: simple algorithm and rapid calculation; besides, it can consider not only the space dependent characteristic but also the time dependent characteristic of the wind history, also, those advantages can be facile to implement by computer programming. Though the autoregressive moving average (ARMA) is superior to the AR model (Samaras, *et al*. 1985, Li and Kareem 1990, Kamal and Jafri 1997, Kho, *et al*. 2002), the parameter estimation for the ARMA model is much more difficult than the AR model (Kizilkaya and Kayran 2006). Hence, this paper still concerns with the issues of the AR model while using it to simulate the natural wind velocity processes.

Before 1980, simulation techniques were primarily adopted to forecast single wind history.

* Corresponding Author, E-mail: yyl_606@yeah.net or gaoweicheng@sina.com

However, the single wind history could not meet the requirements of the structure with a great number of degrees of freedom.

Iwatani (1982) proposed the use of an AR model (multidimensional AR process) to simulate multiple wind velocities firstly (Iwatani 1982). The author built a FORTRAN program and gave out two examples, simulation of shear flow in the vertical direction and simulation of two-dimensional homogenous flow at many points in the horizontal direction, to validate the availability of the AR model. Iannuzzi and Spinelli (1987) compared the methods of simulating both single and multiple wind velocities (Iannuzzi and Spinelli 1987). Huang and Chalabi (1995) used an AR model which could produced non-stationary Gaussian random processes to simulate the wind velocity for the greenhouse and adopted a Kalman filter to estimate the parameters of the AR model (Huang and Chalabi 1995). All these above researchers used algorithms of iteration and recursion which usually result in accumulative errors while calculating the model parameters.

Stathopoulos, Kumar and Mohammadian (1996) established a first-order AR model to simulate the fluctuating wind loads of monoslope roofs with different geometrics (Stathopoulos 1996). Though the first-order AR model was not enough for the complex structures, the study showed that the AR model could be used to analysis the wind-induced responses of the engineering structures. Facchini (1996) used a hybrid model to simulate wind velocity and pointed that the AR model could be calculated directly from the spectral densities without solving the Yule-Walker equations, but it needed huge calculation to obtain covariance functions integrated from the spectral densities of the target processes (Facchini 1996).

Li and Dong (2001) introduced a matrix method to determine the parameters of the AR model without the iteration and recursion, which effectively avoided the accumulative errors in the simulation (Li and Dong 2001). Although the improved method was applied in the simulation of the wind velocity of the double-layer reticulated shell of Chinese National Grand Theater, there were still some incorrectness in reasoning the covariance matrix and some incorrect descriptions of the formula parameters.

Poggi, *et al*. (2003) used an AR model to simulate wind speed in Corsica and compared to the experimental data to check the correction of the simulated wind speed (Poggi, *et al*. 2003). Roy and Fuller (2001) and Kim (2003) discussed the bias of estimators for AR model parameters and evaluated the effects of bias-correction for AR model parameter estimation (Roy and Fuller 2001, Kim 2003).

The wind velocity simulated by numerical simulation methods needs to be as close to the real situation as possible and the simulated method ought to be efficient and general. In the past research, though the AR model was constantly improved, it is not enough for the application of the AR model more widely. The drawbacks of the poor simulated accuracy of the AR model have not been resolved completely yet. Therefore, this paper attempts to deduce the AR model by matrix form and solves the raised issues of the AR model in simulating the wind velocity of the spatial 3-D fields systematically, and presents the corresponding solving methods whose computing programs are implemented in MATLAB.

2. AR model

The fluctuating wind velocity is a random time series in essence, the basic formula of the AR model simulating the wind velocities $[u(t)]$ of M spatial points, which are stationary Gaussian multivariate stochastic processes, can be expressed as (Iwatani 1982, Iannuzzi and Spinelli 1987, Li and Dong 2001):

$$[u(t)] = \sum_{k=1}^{p} [\psi_k][u(t-k\Delta t)] + [N(t)] \tag{1}$$

where $[N(t)] = [N^1(t), \cdots, N^M(t)]^T$, $N^i(t)$ is the i^{th} normally distributed stochastic process with zero mean and unit variance, $i = 1, \cdots, M$, $[\psi_k]$ is the coefficient matrix, $k = 1, \cdots, p$ is the rank of AR model, and Δt is the time step of the series.

The process of the simulation can be delivered as:

2.1. Calculation of coefficient matrix $[\psi_k]$

After multiplying two sides of Eq. (1) by $[u(t-j\Delta t)]$ and calculating the expectation, we can get the following formula:

$$E\{[u(t)][u(t-j\Delta t)]\} = E\left\{\sum_{k=1}^{p} [\psi_k][u(t-k\Delta t)][u(t-j\Delta t)]\right\} + E\{[N(t)][u(t-j\Delta t)]\}$$

Since the covariance between stochastic process $u(t)$ and $u(t-j\Delta t)$ can be expressed as $R_u(j\Delta t) = E[\{u(t)-E[u(t)]\}\{u(t-j\Delta t)-E[u(t-j\Delta t)]\}] = E[u(t)u(t-j\Delta t)]$, and the stochastic process $N(t)$ is independent to stochastic wind velocity $u(t)$, then, the relationship between the covariance $R_u(j\Delta t)$ and the regressive coefficient $[\psi_k]$ can be written as:

$$R_u(j\Delta t) = \sum_{k=1}^{p} [\psi_k] R_u[(j-k)\Delta t] \tag{2}$$

in which $j = 1, 2, \cdots, p$. After transpose, Eq. (2) can be rewritten in the matrix form:

$$[R] = [\bar{R}][\psi] \tag{3}$$

where , $[R]_{pM\times M} = [R_u(\Delta t), \cdots, R_u(p\Delta t)]^T$, $[\psi]_{pM\times M} = [\psi_1^T, \cdots, \psi_p^T]^T$

$$[\bar{R}]_{pM\times pM} = \begin{bmatrix} R_u(0) & R_u(\Delta t) & \cdots & R_u[(p-2)\Delta t] & R_u[(p-1)\Delta t] \\ R_u(\Delta t) & R_u(0) & \cdots & R_u[(p-3)\Delta t] & R_u[(p-2)\Delta t] \\ \vdots & \vdots & \ddots & \vdots & \vdots \\ R_u[(p-2)\Delta t] & R_u[(p-3)\Delta t] & \cdots & R_u(0) & R_u(\Delta t) \\ R_u[(p-1)\Delta t] & R_u[(p-2)\Delta t] & \cdots & R_u(\Delta t) & R_u(0) \end{bmatrix} \tag{4}$$

in which

$$[R_u(j\Delta t)] = \begin{bmatrix} R_u^{11}(j\Delta t) & \cdots & R_u^{1M}(j\Delta t) \\ \vdots & \ddots & \vdots \\ R_u^{M1}(j\Delta t) & \cdots & R_u^{MM}(j\Delta t) \end{bmatrix}, \quad [\psi_j] = \begin{bmatrix} \psi_j^{11} & \cdots & \psi_j^{1M} \\ \vdots & \ddots & \vdots \\ \psi_j^{M1} & \cdots & \psi_j^{MM} \end{bmatrix} \tag{5}$$

According to random vibration theory, the relationship between the power spectral density and the correlation function accords with the Wiener-Khinchin theorem (Strube 1985):

$$R_u^{ik}(j\Delta t) = \int_0^{\infty} S_u^{ik}(f)\cos(2\pi \cdot f \cdot j\Delta t)df \tag{6}$$

in which f is the frequency, $S_u^{ik}(f)$ is the auto-power spectral density if $i = k$, the cross-power spectral density if $i \neq k$, $i, k = 1, 2, \cdots M, j = 1, \cdots, p$.

2.2. Calculation of the normally distributed random processes [$N(t)$]

The normally distributed random processes $[N(t)]$ can be obtained from:

$$[N(t)] = [L][n(t)] \tag{7}$$

where $[n(t)] = [n_1(t), n_2(t), \cdots, n_M(t)]^T$, $n_i(t)$ is the i^{th} independent normally distributed random process with zero mean and unit variance, in which $i = 1, \cdots, M$; $[L]$ is from the Cholesky decomposition of $[R_N] = [L][L]^T$, in which $[R_N]$ is calculated from the following equation obtained by multiplying two sides of Eq. (1) with $[u(t)] = [u^1(t), \ldots, u^M(t)]^T$

$$[R_N] = [R_u(0)] - \sum_{k=1}^{p} [\psi_k][R_u(k\Delta t)] \tag{8}$$

2.3. Calculation of the fluctuating wind velocity

Using the results of Eq. (2) and Eq. (7), with the presumption of $u^i(t) = 0$, while $t < 0$, the Eq. (1) can be dispersed and rewritten as

$$\begin{bmatrix} u^1(h\Delta t) \\ \vdots \\ u^M(h\Delta t) \end{bmatrix} = \sum_{k=1}^{p} [\psi_k] \begin{bmatrix} u^1[(h-k)\Delta t] \\ \vdots \\ u^M[(h-k)\Delta t] \end{bmatrix} + \begin{bmatrix} N^1(h\Delta t) \\ \vdots \\ N^M(h\Delta t) \end{bmatrix}, \quad \begin{matrix} h = 0, 1, 2, \cdots \\ k = 1, \cdots, p \end{matrix} \tag{9}$$

in which Δt is the discrete time step.

2.4. Calculation of the final wind velocity

The final wind velocity can be generated by:

$$V(t) = \bar{v} + u(t) \tag{10}$$

where $\bar{v}$ is the mean component of wind velocity which can be obtained by means of the following logarithmic profile ($z < 100$ m) (Panofsky 1974)

$$\frac{\bar{v}(z)}{\bar{v}(z_1)} = \frac{\ln(z/z_0)}{\ln(z_1/z_0)} \tag{11}$$

where $\bar{v}(z)$ is the mean component of wind velocity with height z, $z_1 = 10$ m is the standard height, z_0 is the roughness length.

2.5. Selection of the AR model rank

Iwatani pointed out that low rank of the AR model can meet the requirements in general engineering with the permitted error (Iwatani 1982). But, for the large and complex structures, it is not credible to solve the rank of AR model based on the empirical analysis only. However, much work has already been done and many experimental results have been given in Schlindwein, and Evans (1990), Akaike (1974), and Pappas, *et al*. (2006) proposed a new method to select the AR(MA) model order by translate the *n*-variate AR model equations into state-space form. Different from those former work, in this study, based on MATLAB programming, a new method of resolving the rank of AR model is developed based on the principle of the AIC(Akaike Information Criterion). The AIC can be expressed as (Akaike 1974)

$$AIC(p) = \ln \sigma_\alpha^2 + 2p / N \tag{12}$$

where N is the sample time length, σ_α^2 is the variance.

With the increasing rank of the AR model initially, the value of the variance σ_α^2 decreases, neither do the value of $AIC(p)$. However, the value of $AIC(p)$ will increase with the rising rank. Hence, p_0 is taken as the best rank of the AR model if it is determined by the formula for a special rank m

$$AIC(p_0) = \min_{1 \le p \le m} AIC(p)$$

It is a huge job to calculate the variance σ_α^2 for a multidimensional sequence. In this paper, the authors propose that the variance σ_α^2 can be replaced by the absolute of the maximum eigenvalue of the matrix $[R_N]$. Then, N becomes the modified model parameter, and $N = 10 \sim 15$ for large span structure. Examples show that it is efficient for ascertaining the rank of the AR model of the multidimensional random sequences.

3. Implementation of the AR model

There are three important points in the implementations of the AR model based on the MATLAB programming (Fig. 1):

3.1. Solving the ill-posed equation (3) resulting from the increasing degrees of freedom of the structure

The Eq. (3) can be solved by a general iterative method for the structure with a few degrees of freedom. However, the large dimension of the coefficient matrix $[R]$, which results from a number of degrees of freedom of the structure, will bring the Eq. (3) to the ill-conditioned equation. Therefore, the complicated method with better accuracy is needed for resolving the problem. Here, over-relaxation iteration (Martins, *et al*. 1996) is used to calculate the large sparse matrix equation.

The iteration formula of the algorithm is

$$\psi_{ij}^{K+1} = (1-\omega)\psi_{ij}^k + \frac{\omega}{r_{ii}}\left[\bar{r}_{ij} - \sum_{l=1}^{i-1} r_{il}\psi_{lj}^{k+1} - \sum_{l=i+1}^{pM} r_{il}\psi_{lj}^k\right] \tag{13}$$

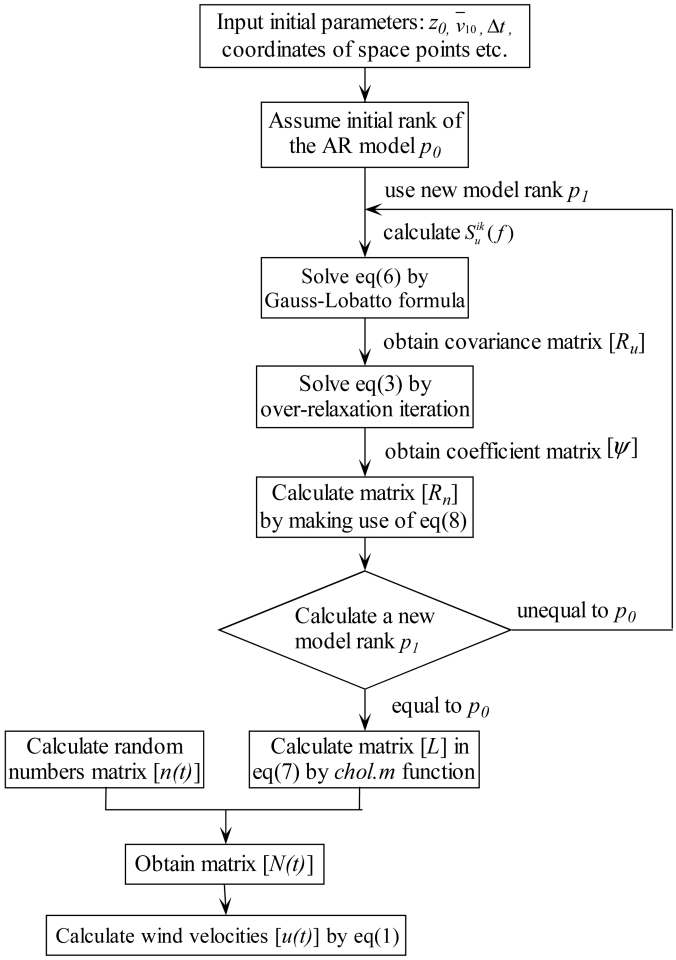

Fig. 1 Flow chart of implementing wind velocity by AR model in MATLAB

where ω is the relaxation factor which controls the convergent rate of the iteration algorithm, $i = 1, 2, \ldots pM$, $j = 1, 2, \cdots M$. With the condition of the positive definite matrix $[R]$, the formula would be convergent with $1 < \omega < 2$. It is suggested that the relaxation factor value should be within the range of 1.01~1.05 in this study.

3.2. Solving the numerical integral equation (6) which contains oscillating function

The integral function of Eq. (6) contains the oscillating function $\cos(2\pi \cdot f \cdot j\Delta t)$. With the growth of the variable $2\pi \cdot j\Delta t$, the integral function will has more points of zero value on x-axis coordinate. Then, a general numerical interpolation can not meet the requirement of accuracy, and neither can the compound integral method. In this study, the Gauss-Lobatto formula improved from the Gauss formula is taken advantaged to solve the integral of oscillation function. The formula can be expressed as (Gander and Gautschi 2000)

$$R_u = A_1 f(a) + A_n f(b) + \sum_{k=2}^{n-1} A_k f(x_k) + K_n f^{(2n-2)}(\xi) \tag{14}$$

where a, b are the endpoints of each range, $A_1, \cdots A_n, K_n$ are $n+1$ parameters.

3.3. Generating the random numbers

The random numbers in the Eq. (7) play very important role in the implementation of the whole algorithm. But, generally, the random numbers generated by the default order in MATLAB are not the real random variables that can result in the non-positive definite matrix $[R_N]$ and the failure of the Cholesky decomposition. With the condition of the enough large sample spaces where the random numbers produce, the numbers would be the random variables as realistic as possible.

The mixed congruence and the central limit theorem of Lindberg-Levy (Gaenssler and Joos 1992) are used to generate the random numbers in this study. The procedure can be expressed as

Step 1 Produce the uniformly distributed random variables with zero mean and unit variance by the method of mixed congruence. The formula of the algorithm can be presented as

$$\begin{cases} x_{n+1} \equiv \lambda x_n + C(\mathrm{mod} M) \\ r_n = \dfrac{x_n}{M_0} \end{cases} \tag{15}$$

where λ is the multiplying factor, M_0 is the modulus, C is a non-negative integer. The statistical character of the produced random numbers can be improved by choosing a proper C which is an odd positive integer smaller than modulus M. This study proposes the values of the parameters: $x_0 = 1$, $\lambda = 5^{19}$, $M_0 = 2^{48}$.

Step 2 Convert the uniformly distributed random variables produced in step 1 into the normally distributed random variables with mean zero and unit variance using the Lindeberg-Levy central limit theorem. In case of some uniformly distributed random variables $\xi_1, \xi_2, \cdots \xi_n$ in (0, 1), then, the variable η below is gradually becoming a normally distributed random variable.

$$\eta = \left(\sum_{i-1}^{n} \xi_i - \frac{n}{2} \right) \Big/ \left(\sqrt{\frac{n}{12}} \right) \tag{16}$$

The number of sample spaces produced by the above method can reach 2^{48} rather than 2^{30} produced by the MATLAB *random.m* function.

4. Examples

4.1. Example 1 four spatial points

Using those methods mentioned above can simulate the wind velocity of the four-space points (Fig. 2). The parameters used in the simulation are: roughness length $z_0 = 0.4$ m, the standard mean component of the wind velocity $\bar{v}_{10} = 25$ m/s, the rank of the AR model $p = 4$, and the discrete time $\Delta t = 0.1$s. The wind velocity power spectrum is the Davenport spectrum. The 3-D spatial

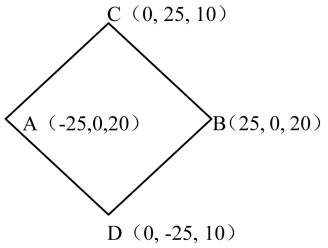

Fig. 2 Four-space points (unit: m)

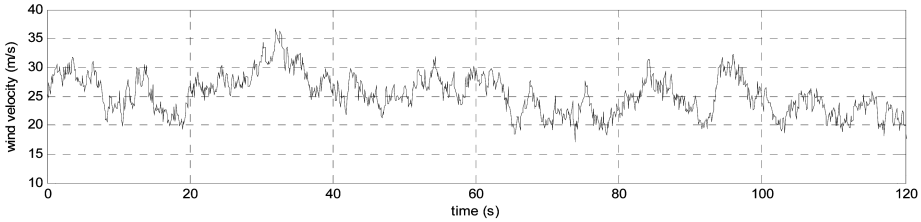

(a) node A

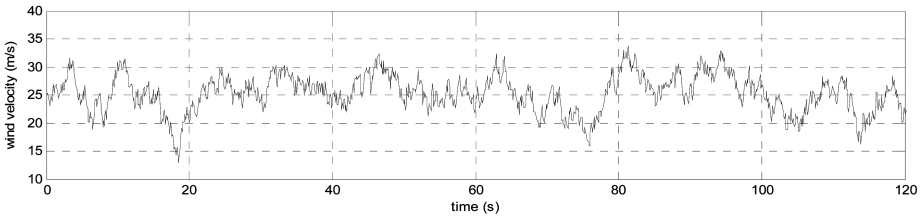

(b) node B

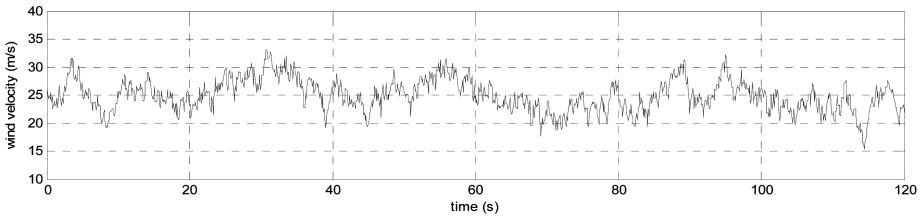

(c) node C

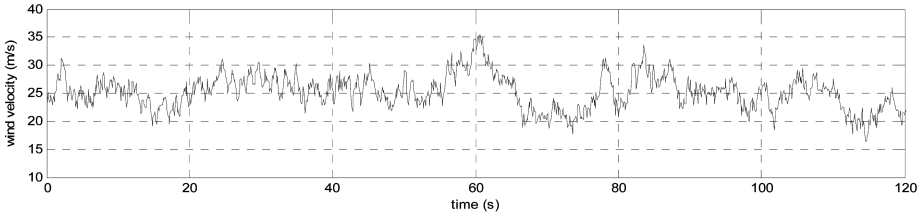

(d) node D

Fig. 3 Wind velocity curves of nodes of example 1

corresponding coefficient related to the frequency of the wind velocity is adopted in the simulation. The same example is applied in Li and Dong (2001). The results of the simulation are shown in Figs. 3 to 5.

Fig. 3 shows the final wind velocities of the four-space points, including the mean and fluctuating components of the wind velocity. The wind velocity curves also illuminate that the wind velocity is a random process accompanying the varieties of time, and the fluctuating components of the wind velocity which displays by the fluctuant curve in Fig. 3 will results in the vibration of the structure, even strengthens the resonance effect of the flexible structure.

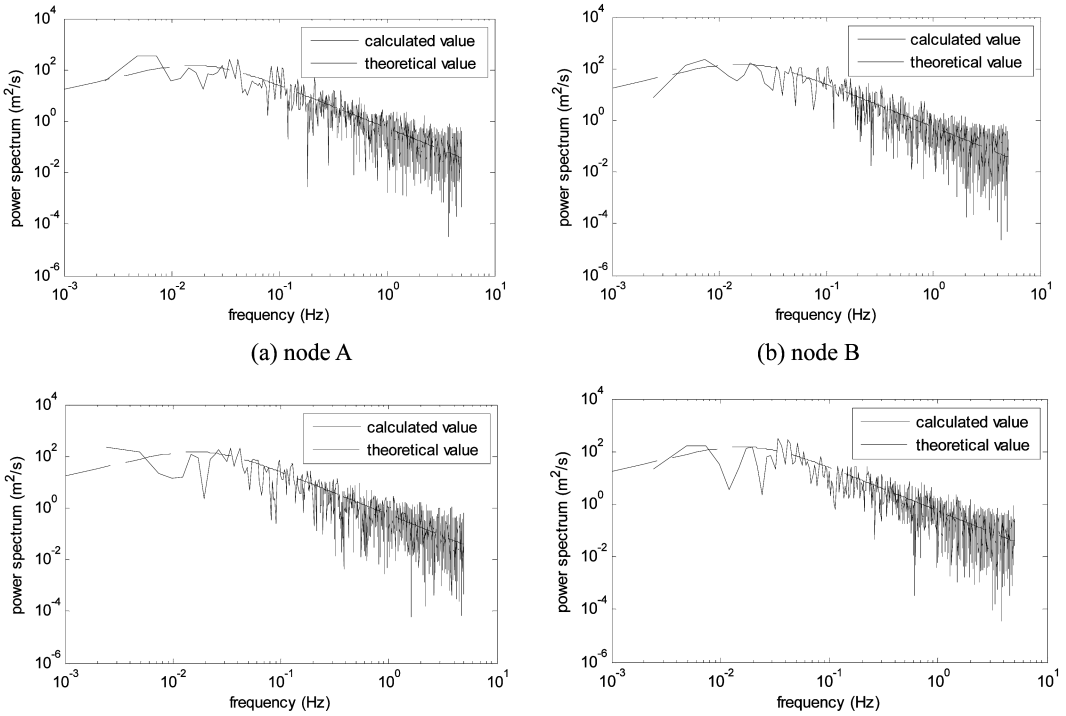

(a) node A (b) node B

(c) node C (d) node D

Fig. 4 Wind velocity power spectral density curves of nodes of example 1

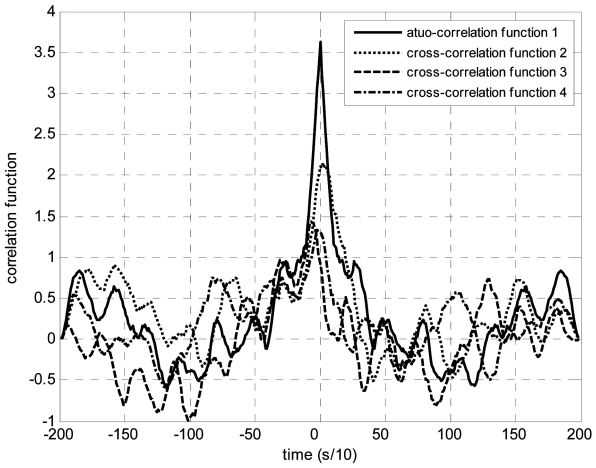

Fig. 5 Correlation functions

Good agreements between the simulated power spectrums and the target power spectrums are shown in Fig. 4. The fluctuant phenomena of the calculated curves result from the fluctuating components of the wind velocity. The beginning and ending of the theoretical values depend on the lower and upper cutoff frequencies respectively. The upper cutoff frequency should be twice larger than the highest natural frequency of the wind velocity.

The auto- and cross-correlation functions in Fig. 5 present the spatial correlation characteristics of the spatial four points. The auto-correlation function 1 is the auto-correlation function of node A; the cross-correlation function 2 is the cross-correlation function between node A and node B; the cross-correlation function 3 is the cross-correlation function between node A and node C; the cross-correlation function 4 is the cross-correlation function between node A and node D. As shown in Fig. 5, the fluctuating curves open out that the wind velocity histories conclude a certain extent of periodicity. However, for most random processes, the relativity is weaker with the longer in time interval and the farther in spatial distance. The correlation function is correlated by itself so as to the maximum value when the time is zero and tends to be zero while the time is infinite. In other words, the closer points in distance have the stronger corresponding properties, in contrast, the farther distance, the weaker corresponding properties.

Fig. 5 also reveals that the relativity among the spatial points with the same height is quite similar. With the fall of height, the maximum of the correlation function will decrease and translate in the negative direction on the time-axis, as described in Wang (1994).

In the above simulation, the rank of the AR model taken in the example is equal to the one in Li and Dong (2001) in order to compare the results. Using the improved AIC mentioned, the rank of the AR model can be newly ascertained by (N=15)

Table 1 Ascertain of AR model rank (Example 1)

Model rank	Values of AIC
p=1	AIC(1)=1.8304
p=2	AIC(2)=1.5260
p=3	AIC(3)=1.4683
p=4	AIC(4)=1.4847
p=5	AIC(5)=1.5684

As shown in Table 1, the rank of the AR model p=3 can meet the accuracy requirement of the wind velocity simulation for the four-space points.

4.1.1. Example 2

A K6-6 type single-layer spherical latticed shell model, with 342 elements and 127 nodes in total, is chosen as an actual engineering example. The node number is shown in Fig. 6. The structural parameters of the shell are: 30m span, rise-span ratio of 1/6, rigidity node constraint, hinged-support boundary constrained linear displacement of three directions only. The type of all poles of the shell is $\Phi 114 \times 4$.

The parameters adopted in the simulation are the same as the ones of the example 1 except for the rank of the AR model.

At first, the rank of the AR model in the simulation of the shell structure, using the improved AIC developed in this paper, is calculated in Table 2 (N=15). As shown by the data in Table 2, the rank of the AR model $p = 5$ is the most suitable value of the wind velocity simulation for the K6-6 type

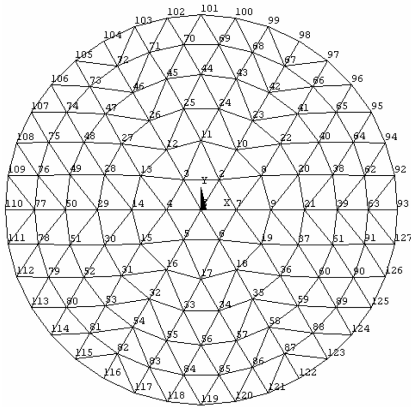

Fig. 6 Node number of K6-6 single-layer spherical latticed shell model

Table 2 Ascertain of AR model rank (Example 2)

Model rank	Values of AIC
p=1	AIC(1)=4.5772
p=2	AIC(2)=4.8891
p=3	AIC(3)=4.5392
p=4	AIC(4)=3.1897
p=5	AIC(5)=2.0064
p=6	AIC(6)=2.0201

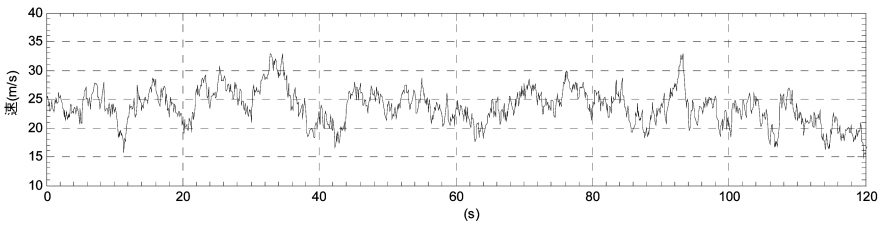

(a) node 3

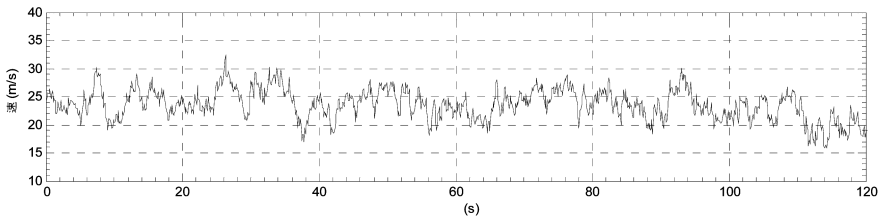

(b) node 31

Fig. 7 Wind velocity curves of nodes of latticed shell

single-layer spherical latticed shell.

The results of the simulation are shown in Figs. 7 to 9.

Fig. 7 shows the final wind velocities of the K6-6 type single-layer spherical latticed shell, including the mean and fluctuating components of the wind velocity.

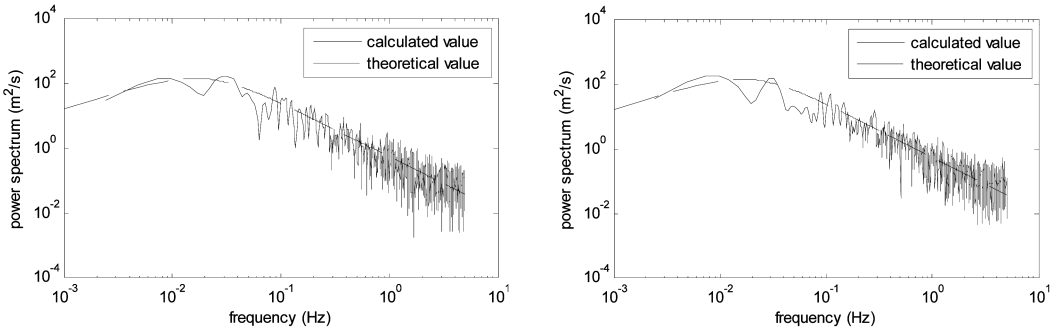

(a) node 3 (b) node 31

Fig. 8 Wind velocity power spectral density curves of nodes of latticed shell

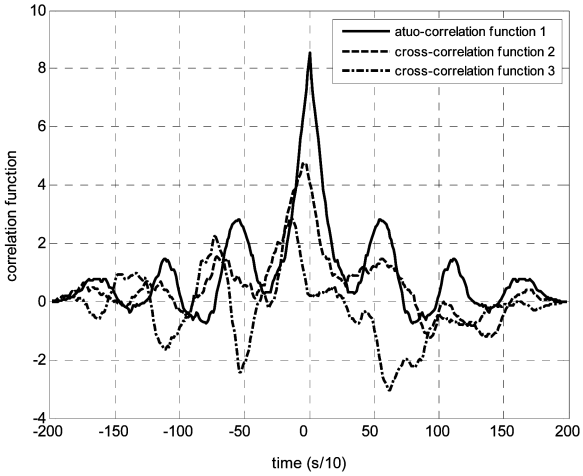

Fig. 9 Correlation functions

Good agreements between the simulated power spectrums and the target power spectrums are shown in Fig. 8. The upper cutoff frequency should also be twice larger than the highest natural frequency of the wind velocity.

The auto- and cross-correlation functions in Fig. 9 also reflect the spatial correlation characteristics of the K6-6 type single-layer spherical latticed shell well. The phenomenon in Fig. 9 is similar to the Fig. 5. The auto-correlation function 1 is the auto-correlation function of node 63; the cross-correlation function 2 is the cross-correlation function between node 63 and node 37; the cross-correlation function 3 is the cross-correlation function between node 63 and node 33.

4.1.2. Example 3

A cable net structure composed of four pieces of hyperbolic paraboloid saddle cable net is chosen as the more complex engineering structure. The horizontal projection size of the structure is 120 m ×120 m, and the height of the structure is 30 m. The sketch map of the structure is shown in Fig. 10. The node number of the cable net model is presented in Fig. 11. The height of the basement of the structure is 10 m.

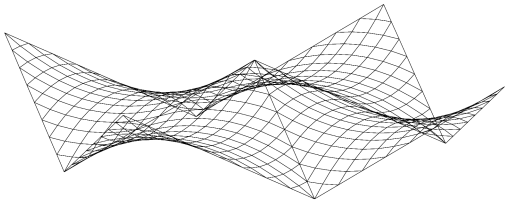

Fig. 10 Cable-net structure model

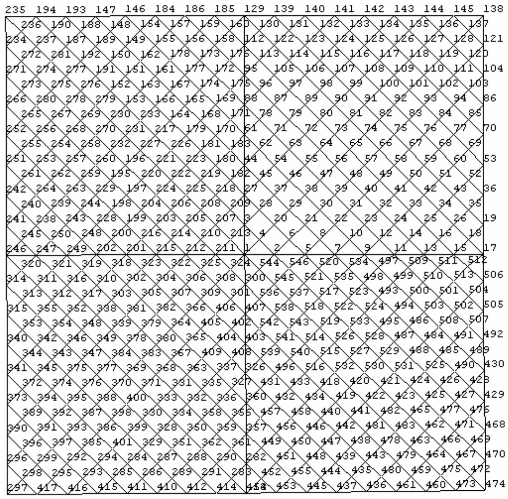

Fig. 11 Node number of cable-net model

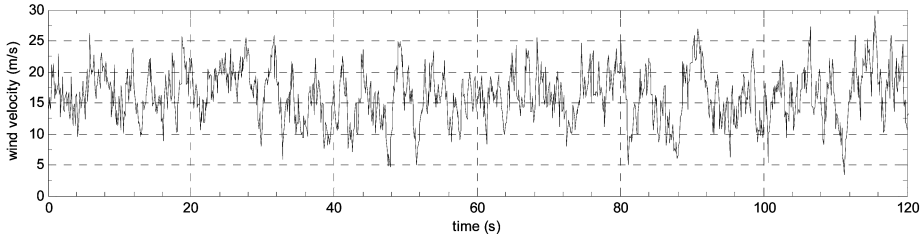

Fig. 12 Wind velocity curve of node 29

The parameters selected in the simulation are: the roughness length $z_0 = 0.01$ m, $\bar{v}_{10} = 16$m/s, and the discrete time $\Delta t = 0.1$ s. The wind velocity power spectrum is the Panofsky spectrum. The 3-D spatial corresponding coefficient, which is independent of the frequency of the wind velocity, is used in the simulation. The rank of the AR model $p = 5$, using the improved AIC developed in this study, is ascertained firstly. The results of the simulation are shown in Figs. 12 to 14.

Fig. 12 shows the final wind velocity of the cable net structure, including the mean and fluctuating components of the wind velocity.

A good agreement between the simulated power spectrum and the target power spectrum is shown in Fig. 13. The upper cutoff frequency should also be twice larger than the highest natural frequency of the wind velocity.

The auto- and cross-correlation functions in Fig. 14 also reflect the spatial correlation characteristics

of the cable net structure perfectly. The auto-correlation function 1 is the auto-correlation function of node 29; the cross-correlation function 2 is the cross-correlation function between node 29 and node 74; the cross-correlation function 3 is the cross-correlation function between node 29 and node 119.

The cross-correlation functions in Fig. 15 are the theoretical and simulated cross-correlation

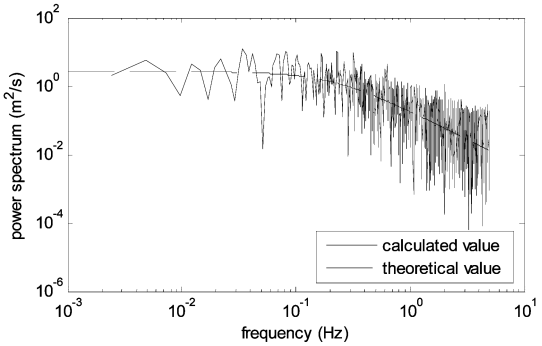

Fig. 13 Wind velocity power spectral density curve of node 29

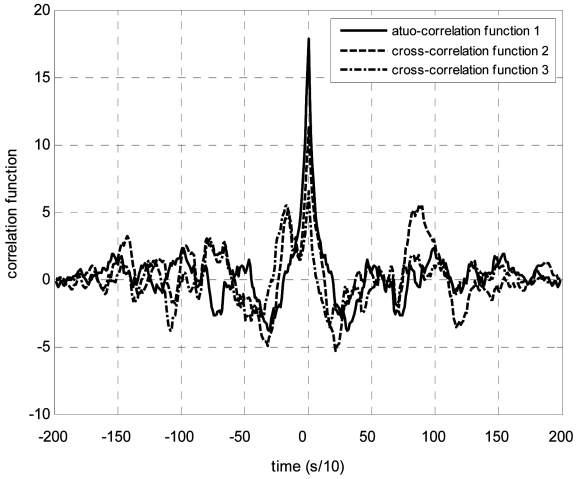

Fig. 14 Correlation functions

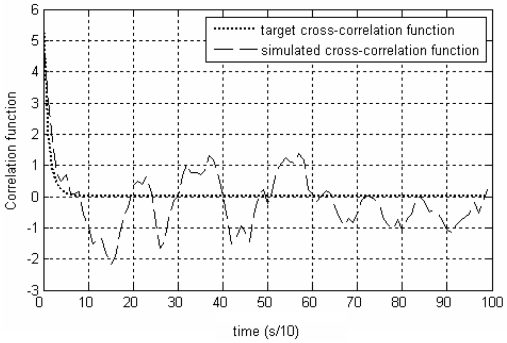

Fig. 15 Verification of correlation function

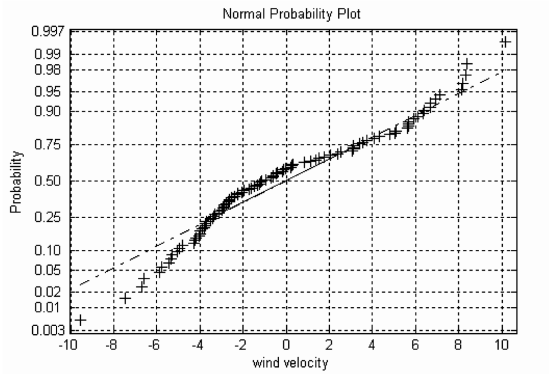

Fig. 16 Normal distribution probability function of wind velocity simulated by unimproved AR model

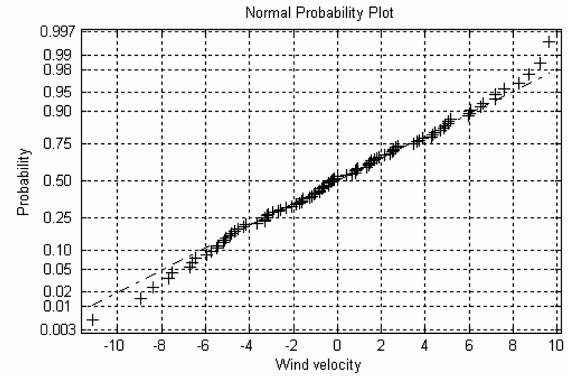

Fig. 17 Normal distribution probability function of wind velocity simulated by improved AR model

functions of wind velocity between node 29 and node 34. It also shows a good agreement between two curves. From the Fig. 15, we can also see that the maximum value of the cross-correlation function is slightly smaller than the cross-correlation function 3 in Fig. 14. This means that the spatial correlation of node 29 and node 34 is weaker than the correlation of node 29 and node 74, which due to the farther distance between node 29 and node 34.

5. Comparisons

Fig. 16 and 17 show the normal distribution probability functions of wind velocity simulated by unimproved and improved AR model respectively. The lines in the Figures mean the data come from the normal distribution strictly, the "+" symbols display the discrete points of simulated wind velocity. As we known, the real wind velocity is subjected to standard normal distribution in nature. From fig.16 and 17, we can see the wind velocity simulated by improved AR model fits the line better than the unimproved model's. The poor simulated accuracy of the AR model had been ameliorated distinctly.

6. Conclusions

The methods discussed in the simulation of wind velocity using the AR model meliorate the accuracy of the AR model and can also be easily adopted in other similar problems by other wind velocity simulation methods, and the method of ascertaining the rank of the AR model is proved to be effective and credible for the wind velocity simulation of the spatial 3-D fields in terms of the examples taken in this paper.

The results of the comparison among power spectral densities are found to be in a very close agreement. The correlation functions reveal the spatial and time correlation characteristics of the wind velocity well.

The built programs can simulate the wind velocity of the spatial 3-D fields for all kinds of wind velocity power spectrums and spatial corresponding coefficients, and afford the fluctuating wind load in the wind induced oscillation numerical analysis of the large structure in civil engineering.

Acknowledgements

The authors wish to express their thanks to Prof. Guang-chun Zhou for his critical reading and constructive suggestion. Funding was provided by the National Nature Science Foundation of China (50478030). The authors would particularly like to thank those people who participated in the precious research included in Refs.

References

Samaras, E., Shinozuka, M. and Tsurui, A. (1985), "ARMA representation of random vector processes", *J. Eng. Mech., ASCE*, **111**(3), 449-461.
Li, Y. and Kareem, A. (1990), "ARMA representation of wind field", *J. Wind Eng. Ind. Aerodyn*., **36**, 415-427.
Kamal, L, and Jafri, Y. Z. (1997), "Time series models to simulate and forecast hourly averaged wind speed in Quetta, Pakistan", *Solar Energy*, **61**(1), 23-32.
Kho, S., Baker, C. and Hoxey, R. (2002), "POD/ARMA reconstruction of the surface pressure field around a low rise structure", *J. Wind Eng. Ind. Aerodyn*., **90**, 1831-1842.
Kizilkaya, A. and Kayran,A. H. (2006), "ARMA model parameter estimation based on the equivalent MA approach", *Digit. Signal Process*., **16**, 670-681.
Iwatani, Y. (1982), "Simulation of multidimensional wind fluctuations having any arbitrary power spectra and cross spectra", *J. Wind Eng*., **11**, 5-14. (in Japanese)
Iannuzzi, A. and Spinelli, P. (1987), "Artificial wind generation and structural response", *ASCE, J. Struct. Eng*., **113**(10), 2382- 2398.
Huang, Z. and Chalabi, Z. S. (1995), "Use of time-series analysis to model and forecast wind speed", *J. Wind Eng. Ind. Aerodyn*., **56**, 311-322.
Stathopoulos, T., Kumar, K. S. and Mohammadian, A. R. (1996), "Design wind pressure coefficients for monoslope roofs: A time series approach", *J. Wind Eng. Ind. Aerodyn*., **65**, 143-153.
Facchini, L. (1996), "The numerical simulation of Gaussian cross-correlated wind velocity fluctuations by means of a hybrid model", *J. Wind Eng. Ind. Aerodyn*., **64**, 187-202.
Li, Y-Q. and Dong, S-L. (2001), "Random wind load simulation and computer program for large-span spatial structures", *Spatial Structure*, **7**(3), 3-11.(in chinese)
Poggi, P., Muselli, M., Notton, G., Cristofari, C. and Louche, A. (2003), "Forecasting and simulating wind speed in Corsica by using an autoregressive model", *Energ Convers. Manage*., **44**, 3177-3196.
Roy, A. and Fuller, W. A. (2001), "Estimation for autoregressive time series with a root near one", *J. Bus Econ Stat*., **19**, 482-493.
Kim, J. H. (2003), "Forecasting autoregressive time series with bias-corrected parameter estimators", *International J. Forecasting*, **19**, 493-502.
Strube, H. W. (1985), "A generalization of correlation functions and the Wiener-Khinchin theorem", *Signal Process*, **8**(1), 63-74.
Panofsky, H. A. (1974), "The atmospheric boundary layer below150 meters", *Ann Rev. Fluid Mech.*, **6**, 147-177.
Schlindwein, F. S. and Evans, D. H. (1990), "Selection of the order of autoregressive models for spectral analysis of Doppler ultrasound signals", *Ultrasound Med. Biol*. **16**(1), 81-91.
Akaike, H. (1974), "A new look at the statistical model identification", *IEEE Trans. Automatic Control*, **19**, 716-723.
Pappas, S. S., Leros, A. K. and Katsikas S. K. (2006), "Joint order and parameter estimation of multivariate autoregressive models using multi-model partitioning theory", *Digit Signal Process*, **16**, 782-795.
Martins, M. M., Trigo, M. E. and Santos. M. M. (1996), "An error bound for the SSOR and USSOR methods", *Linear Algebra. Appl*., **232**, 131-147.
Gander, W. and Gautschi, W. (2000), "Adaptive quadrature revisited", *Numer Math.*, **40**, 84-101.
Gaenssler, P. and Joos, K. (1992), "Another view on martingale central limit theorems", *Stoch. Proc. Appl.*, **40**(2), 181-197.
Wang, Z-H. (1994), "Simulation of wind loading", *J. Build. Struct.*, **15**(1), 44-52. (in chinese)